Iran Polym J (2014) 23:891–898
DOI 10.1007/s13726-014-0288-x

ORIGINAL PAPER

Self-healing and anticorrosive properties of Ce(III)/Ce(IV) in nanoclay–epoxy coatings

I. Danaee · E. Darmiani · G. R. Rashed · D. Zaarei

Received: 1 May 2014 / Accepted: 5 October 2014 / Published online: 15 October 2014

Abstract The self-healing and anticorrosion effects of cerium nitrate in epoxy–clay nanocomposite coatings systems were studied. Different amounts of cerium (III) were added to epoxy–montmorillonite clay composites and the nanocomposite coatings were prepared and applied on cold rolled steel panels. Ultrasonication was applied to disperse the nanoclay into the epoxy cerium nitrate composition. Electrochemical impedance spectroscopy (EIS) was used to study the self-healing and anticorrosion behaviors of the coatings. The structure of the dry coating and the protective mechanism of the pigments in the coating were investigated by scanning electron microscopy (SEM), energy dispersive X-ray spectroscopy (EDX) analysis and field emission electron microscopy (FESEM). Transmission electron microscopy (TEM) illustrated the separation of clay layers which interacted with the epoxy resin. Electrochemical impedance data indicated that the epoxy cerium (III)–montmorillonite nanocomposite coatings were superior to the epoxy coatings in corrosion protection properties. The self-healing behavior of such coatings was due to the presence of cerium nitrate that could be released at the defects within the coating and hindered the corrosion reactions at the defective sites. It was shown that the best corrosion protection was achieved with nanocomposite coatings containing 4 wt% clay and 2 wt% cerium nitrate.

I. Danaee (✉) · E. Darmiani · G. R. Rashed
Abadan Faculty of Petroleum Engineering, Petroleum University of Technology, Abadan, Iran
e-mail: danaee@put.ac.ir

D. Zaarei
Technical Faculty South Tehran Branch, Islamic Azad University, Tehran, Iran

Keywords Nanocomposite · Montmorillonite · Ce(III)/Ce(IV) · Corrosion · Impedance

Introduction

Many researchers have used various kinds of additives such as extenders and inorganic pigments to enhance the barrier properties of polymeric coatings [1, 2]. In comparison to conventional pigments, addition of nanoparticles into polymeric coatings offers a more economical method and provides more durable protection against corrosion [3]. With the addition of small amount of the nanofillers into different polymer matrices, the nanocomposite coatings show substantial increases in various physical and chemical properties, including thermal stability, mechanical properties, flame retardancy, barrier resistance, solvent resistance and electro-rheology properties [4–6].

In recent years, clay, a non-toxic, cheap, available and environmentally friendly additive, has been commonly used for fabrication of nanocomposite coatings. Investigations indicated that the incorporation of a little amount of clay (1–5 %) into the coating formulations could increase the anticorrosive, barrier, thermal and mechanical properties and decrease permeability to liquids and gases [7, 8]. The optimum nanoclay content was reported between 2 and 5 wt% in different studies [9, 10].

For a long time, chromate compounds (Cr^{6+}) have been used as effective and inexpensive corrosion inhibitors for different alloys and coatings [11]. However, with the advent of increasing environmental awareness, the toxicity and carcinogenic nature of Cr^{6+} base treatment have made its use undesirable [12]. New alternatives and environmental corrosion inhibitors need to be developed. Rare earth salts have been successfully used for the corrosion protection of

many metals and alloys in aqueous environments [13–15]. The use of the rare earth salts to form conversion films as dopants in sol–gel or multifunctional silane pre-treatments is another way of achieving corrosion protection.

It has been reported [14, 15] that cerium salts decrease the corrosion rate of aluminum by inhibiting cathodic reactions. These works have proposed that the cathodic reactions (oxygen reduction and hydrogen evolution) may generate an alkaline environment that leads to the precipitation of rare earth oxides and forms a protective surface film. Furthermore, the rare earth film possesses good self-healing properties [16–18]. Montemor et al. [19, 20] have studied the effect of treatment time on the chemical composition and corrosion behavior of $Ce(NO_3)_3$ conversion coatings for galvanized steel and found that the film composition and the thickness change with time.

Nevertheless, the self-healing effect of cerium has not been studied in nanocomposite coatings such as epoxy. The aim of this study was to evaluate the self-healing ability of cerium (III)/cerium (IV) and its anticorrosive behaviors on montmorillonite nanocomposite coatings. The dispersion morphology and the degree of agglomeration were evaluated by TEM and FESEM. The electrochemical impedance spectroscopy (EIS), polarization measurement, SEM and EDX were used to investigate the anticorrosive and self-healing properties of nanocomposite coatings.

Experimental

Cerium (III) nitrate was provided from Scharau (Spain). Epoxy resin and its hardener (F-206) were prepared from Bajak paint Co. (Iran). The organically modified montmorillonite clay (Cloisite 20A; dimethyl, dehydrogenated tallow, quaternary ammonium modified montmorillonite) was supplied by Southern Clay Products, Inc. (USA) with particle size of 2–13 μm and layer thickness of 1 nm. The clay particles were dried at 80 °C for 24 h. Ethanol was provided by Merck.

Montmorillonite clay was dispersed into the epoxy resin via mechanical mixing and sonication. Also, cerium nitrate in different amounts was dissolved in ethanol. The added amounts of particles were based on the weight percent of the solid part of paints. The paints-designated samples were according to the weight percent of the particles added to the formulation. Therefore, 0C0CN illustrated composite coating containing 0 wt% clay and 0 wt% cerium nitrate. Cerium nitrate-modified ethanol and epoxy containing montmorillonite were mechanically mixed at 1200 rpm and then the mixture was subjected to sonication for 40 min and afterward the hardener was added. SAE 1010 carbon steel panels were blasted to Sa 2 1/2 (SIS 055900-1967) with a profile of 15–25 μm and then degreased with toluene and acetone. A film applicator was used for coatings. The dry film thickness (DFT) was measured by Elcometer 415 and was found to be 60 ± 10 μm for all panels. To ensure the films' curing, the panels were kept in a laboratory atmosphere for a week before beginning the tests.

Scanning electron microscopy (Vega Tescan) with EDX-detector was utilized to investigate the structure of the dry prepared coating and the protective mechanism of the pigment and coating. The operating voltage applied in the SEM analysis was 15 kV.

A Hitachi field emission scanning electron microscopy (FESEM) model S4160 was used to study the film properties. Technics Hummer II SEM Sputtering System was used for implementation of Au coating on samples.

The TEM specimens were cut from nanocomposite blocks using an ultra-microtome, OMU3 (Reichert, Austria), equipped with a diamond knife. Thin specimens (70–100 nm) were cut from cured film of the nanocomposites materials of about 1 × 1 mm^2. The samples were placed on 300 mesh copper grids. Transmission electron micrographs were obtained by a Philips-EM208 at an acceleration voltage of 100 kV.

The electrochemical impedance spectroscopies (EIS) were measured at room temperature in a Faraday cage using a frequency response analyzer (FRA). A three-electrode electrochemical cell was used, consisting of the coated steel as working electrode (3.15 cm^2 of exposed area), a saturated Ag/AgCl as reference electrode and platinum as counter electrode. The measuring frequency ranged from 100 kHz to 20 MHz with AC amplitude of 10 mV. The interpretation of impedance data was done using Autolab frequency response analyzer software.

Results and discussion

FESEM and TEM

To study the visual morphology of nanoclay, field emission scanning electron microscopy (FESEM) test was conducted. Figure 1 presents the FESEM of clay before dispersion in the coating compositions. This analysis indicated that the clay sheets were in the form of cauliflower shape with an approximate dimension of 1,000–1,500 μm, and that clay plays a role on the barrier effect.

Figure 2a presents the surface morphology of the film containing cerium nitrate. It can be seen that the film is not continuous. Several microcracks and pinholes are observed on the coating. These defects were treated by the addition of clay into the matrix and are shown in Fig. 2b. Clay seems to have filled the microcracks and pinholes and improved the film. Also, it hindered the penetration of aggressive

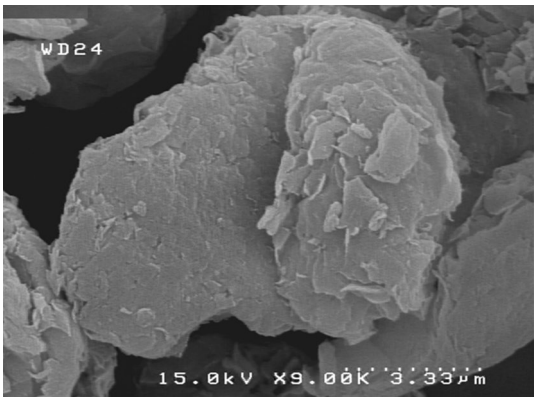

Fig. 1 FESEM images of Cloisite 20A clay

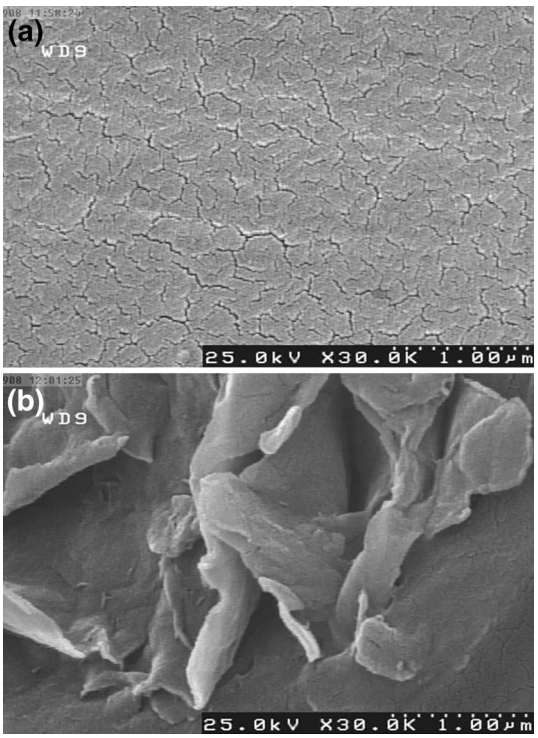

Fig. 2 FESEM surface morphology of unexposed sample 0C3CN (**a**) and 4C2CN (**b**)

species toward the metallic substrate as a physical barrier and enhanced the anticorrosion behavior.

Figure 3 illustrates the TEM image of the epoxy–clay nanocomposite. Some individual crystallites of the silicate are observed as regions of alternating narrow, dark and light bands within the particles and resin. The separation of clay layers revealed the intercalation of clay layers [21]. This figure also shows some clay sheet separations with more than 9 nm, which have resulted in partial exfoliated dispersion. Platelet spacing is evident from TEM images

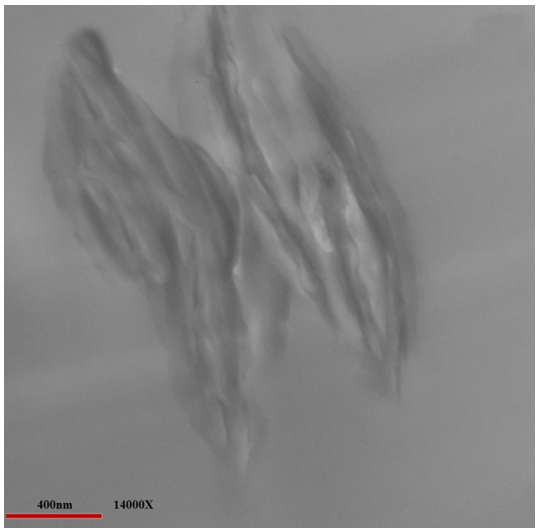

Fig. 3 TEM photos of nanocomposite of 4C2CN

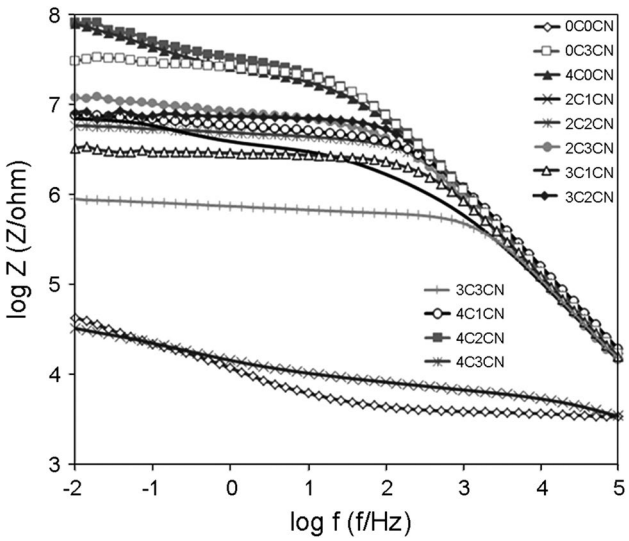

Fig. 4 Representative Bode diagrams for different coated samples after 100 days' immersion

which confirm the FESEM results. Thus, it can be concluded that the MMT platelets in 4C2CN interact with resin and intercalate, but generate a small amount of tactoids or clay ordered structures in the matrix.

Electrochemical study

Optimal formulation of epoxy cerium nitrate–montmorillonite nanocomposite coating

To investigate the anticorrosion properties of coatings with respect to time, electrochemical impedance spectroscopy (EIS) was performed when exposed to a 3.5 wt% NaCl

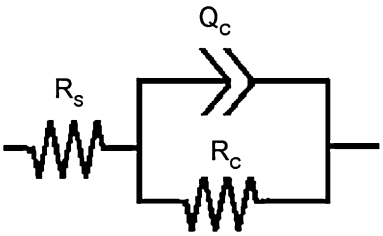

Fig. 5 Equivalent circuits compatible with the experimental impedance data in Fig. 4 for different nanoclays and cerium nitrate in different immersion times

Table 1 The electrochemical parameters measured from the EIS plots of the epoxy cerium nitrate–montmorillonite nanocomposite as a function of exposure time and concentration of nanoparticles after (a) 1 h immersion and (b) 100 days' immersion

	R_C (Ω)	Q_C (F)
(a) Test samples 1 h		
0C0CN	3.98×10^5	2.26×10^{-6}
0C3CN	8.07×10^6	1.19×10^{-9}
4C0CN	5.54×10^8	3.85×10^{-10}
2C2CN	2.28×10^8	3.51×10^{-10}
3C2CN	1.15×10^9	2.78×10^{-10}
4C2CN	1.59×10^9	5.06×10^{-10}
(b) Test samples 100 days		
0C0CN	3.17×10^4	3.37×10^{-5}
0C3CN	5.87×10^7	1.44×10^{-9}
4C0CN	2.10×10^7	4.38×10^{-10}
2C2CN	7.99×10^4	5.08×10^{-10}
3C2CN	2.57×10^7	8.84×10^{-10}
4C2CN	4.07×10^7	1.20×10^{-10}

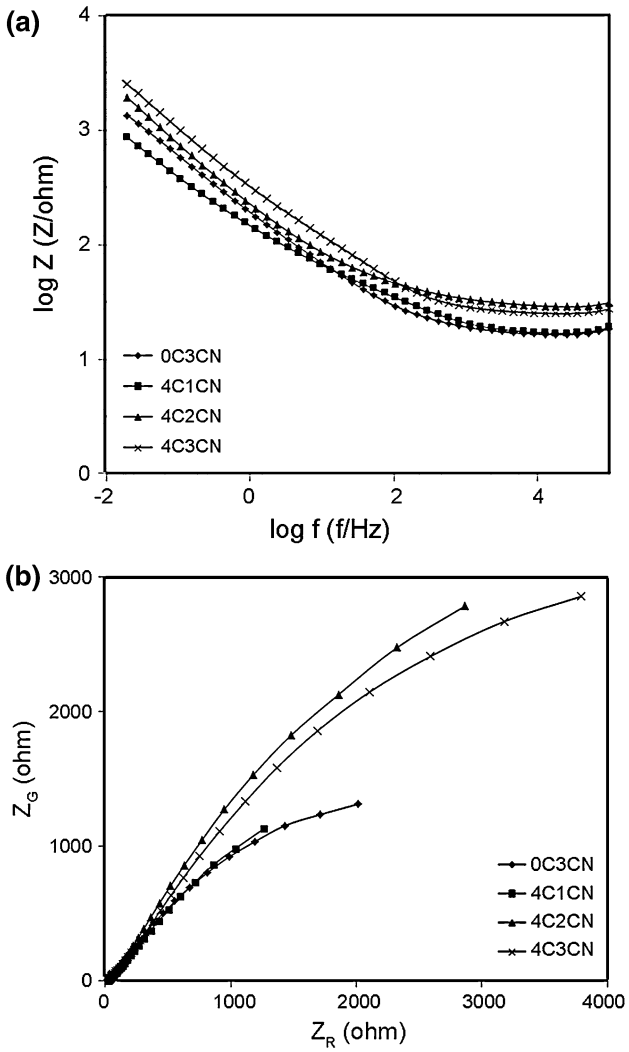

Fig. 6 **a** Bode and **b** Nyquist diagrams for different scratched coating samples after 1 day of immersion

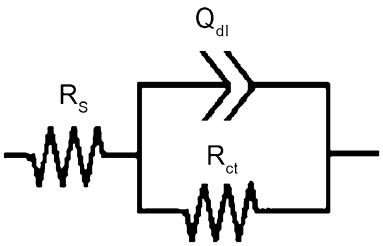

Fig. 7 Equivalent circuits compatible with the experimental impedance data of scribed coatings in Fig. 6 for different nanoclays and cerium nitrate in different immersion times

solution. Figure 4 presents the Bode diagram for all samples after 100 days of immersion. Impedance diagrams display the resistance and capacitance profile of polymer coating. The general equivalent circuit compatible with the Bode diagrams is depicted in Fig. 5. To obtain a satisfactory impedance simulation, it was necessary to replace the capacitor (C) with a constant phase element (CPE) Q in the equivalent circuit. Constant phase element Q_c, R_s and R_c can be related to the coating layer capacitance, solution resistance and coating resistance, respectively. The most widely accepted explanation for the presence of CPE behavior and depressed semi-circles on solid electrodes is microscopic roughness, causing an inhomogeneous distribution in the solution resistance as well as in the double layer capacitance [22, 23]. To corroborate the equivalent circuit, the experimental data were fitted to the equivalent circuit and the circuit elements were obtained. Table 1 shows the data of the equivalent circuit parameters compatible with the impedance spectra for different immersion times, 1 h and 100 days. As indicated in Table 1, the coating capacitance increased from 2.26 to 33.7 μF. This can be due to water absorption, as water has a higher dielectric constant with respect to the polymeric

coatings [10]. In addition, loading of MMT and CN into the epoxy coating led to increasing the pore resistance during the long period of immersion time in corrosive solution. Higher values of R_C mean higher corrosion protection and lower ion permeability through the coating. Plates-like structure of MMT nanoparticles was incorporated into the polymer matrix and made a barrier layer in the polymeric matrix. This behavior could prevent the penetration of electrolyte through the coating and therefore increase the corrosion resistance [24]. This was attributed to the greater area to thickness ratio of MMT, which led to traveling a longer tortuous path for corroding agents to reach the substrate [25]. The ion permeability depended on the length, orientation, and degree of delamination of layered silicates [25]. As the dispersion and delamination of clay layers appeared in the TEM, better corrosion protection was predictable due to the blocking of the pores and defects of these coatings.

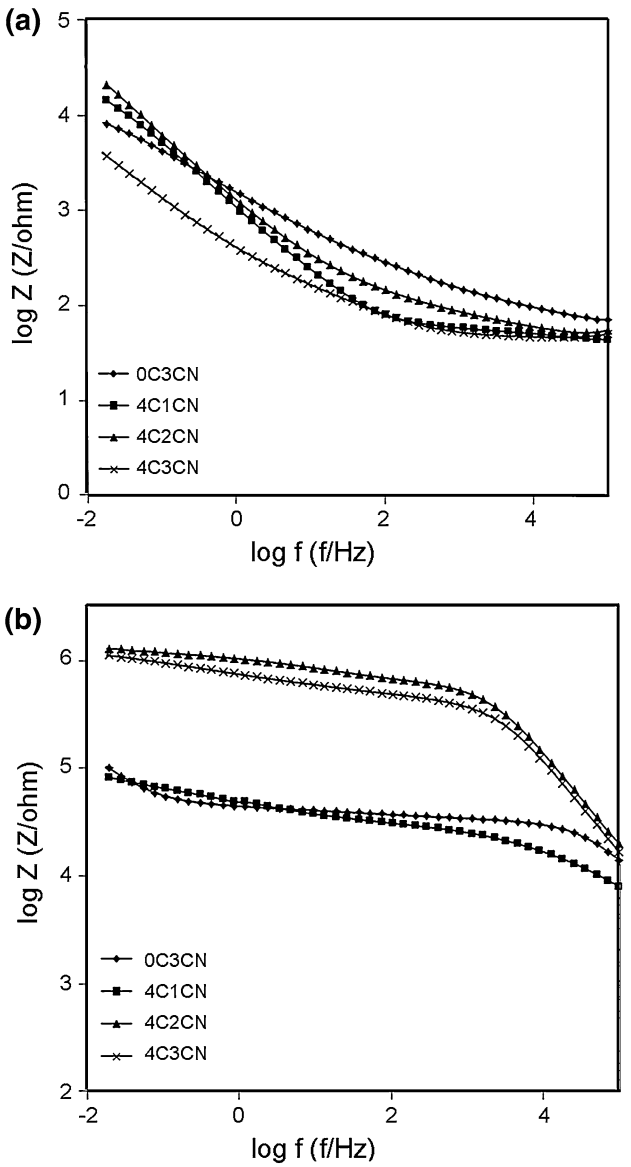

Fig. 8 Bode diagrams for different scratched coating samples after: (**a**) 12 days of immersion and (**b**) 27 days of immersion

Investigation of the healing ability of cerium nitrate in the epoxy–clay matrix

To study the leaching and healing abilities of cerium nitrate in the epoxy matrix, the prepared coatings with 0C3CN, 4C1CN, 4C2CN and 4C3CN compositions were scratched and then immersed in 3.5 wt% NaCl solutions for 27 days. Figure 6 indicates the Bode phase and Nyquist plots after 1 day immersion, which shows one time constant due to the double layer capacitance and charge transfer resistance. As can be seen, higher charge transfer resistance was obtained for 4C2CN and 4C3CN samples. Figure 7 shows the equivalent circuit compatible with impedance diagrams. The capacitor (C) was replaced by a constant phase element (CPE) Q in the equivalent circuit. Constant phase elements Q_{dl} and R_{ct} can correspond to the double layer capacitance, $Q_{dl} = R^{n-1}C_{dl}^{n}$ [26], and charge transfer resistance, respectively. The experimental impedance diagrams in higher immersion times are shown in Fig. 8 and the impedance parameters for different exposure times 1, 12 and 27 days are presented in Table 2. As can be seen, R_{ct} for all samples increases with exposure time. It seems that the intermediate oxide layer has healed with time, showing the "self-healing" ability of the films. The deposition of cerium oxides and hydroxides within the intermediate oxide layer block the cracks and causes the "self-healing" ability.

Table 2 The electrochemical parameters measured from the EIS plots of the scratched coating samples as a function of exposure time and concentration of nanoparticles after (a) 1 day of immersion, (b) 12 days of immersion and (c) 27 days of immersion

	R_{ct} (Ω)	Q_{dl} (F)
(a) Test samples 1 days		
0C3CN	6.11×10^{3}	2.41×10^{-3}
4C1CN	5.52×10^{3}	3.05×10^{-3}
4C2CN	1.31×10^{4}	7.22×10^{-4}
4C3CN	1.27×10^{4}	4.44×10^{-4}
(b) Test samples 12 days		
0C3CN	2.71×10^{4}	1.55×10^{-4}
4C1CN	3.23×10^{4}	2.23×10^{-4}
4C2CN	8.41×10^{4}	1.11×10^{-4}
4C3CN	2.25×10^{4}	4.14×10^{-4}
(c) Test samples 27 days		
0C3CN	3.05×10^{5}	3.62×10^{-5}
4C1CN	3.22×10^{5}	8.74×10^{-5}
4C2CN	1.27×10^{6}	2.87×10^{-5}
4C3CN	1.08×10^{6}	1.66×10^{-5}

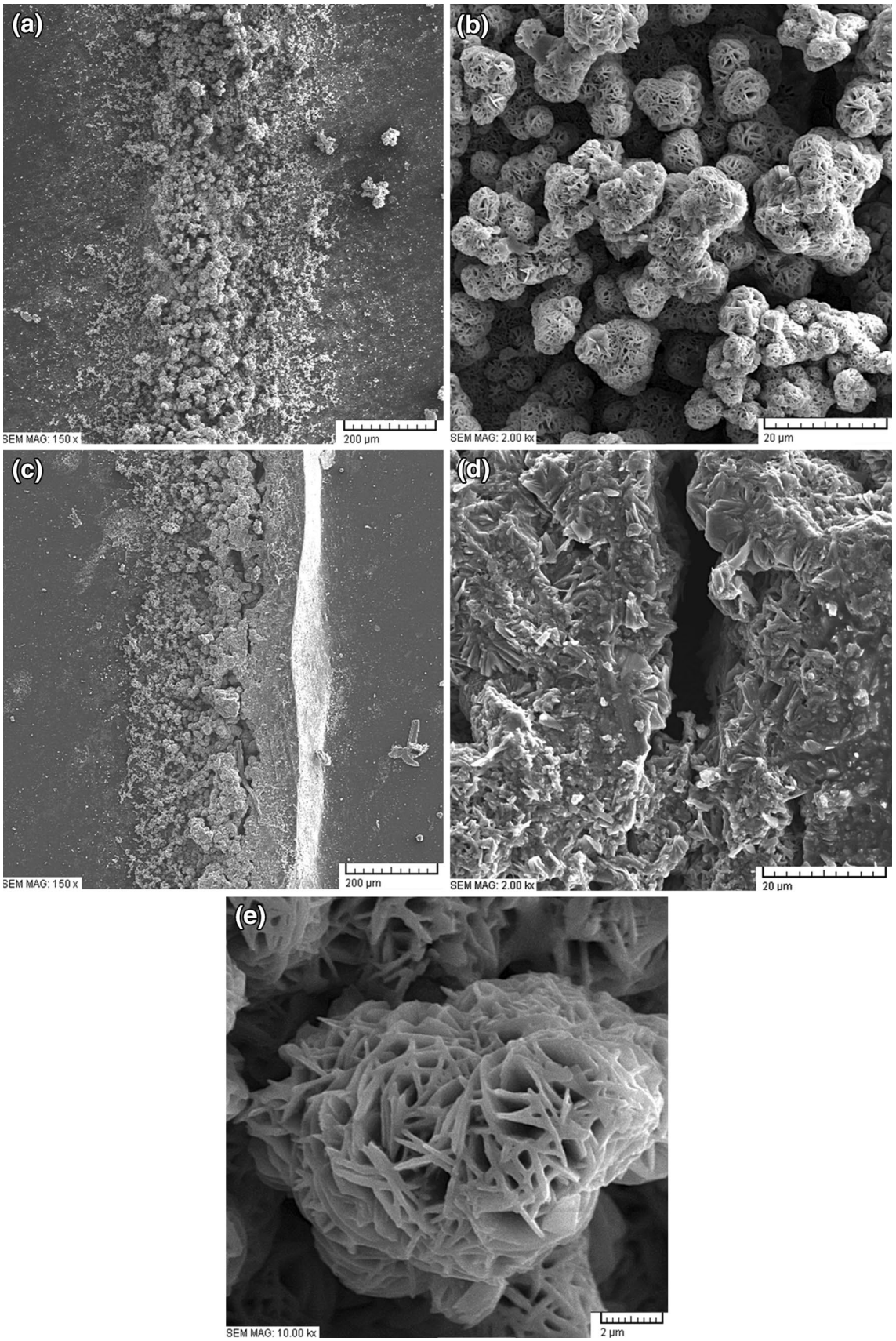

Fig. 9 SEM micrograph from the scratch area for samples 4C2CN (**a**) and (**b**) and for sample 4C3CN (**c**), (**d**) and (**e**) in different magnifications

Ce^{4+} is moderately soluble, whereas Ce^{3+} remains in an insoluble state [25]. The cathodic reaction in the coating led to oxidation of the cerium 3+ ions to cerium 4+. Subsequently, the moderately soluble Ce^{4+} ions are released from the coating. In addition, bare metal reduces the Ce^{4+} to Ce^{3+} state and forms the hydroxide/oxide layer, which protects the bare metal from further corrosion [10, 27]. Ce^{4+} is in the form of $Ce(OH)_2^{2+}$ as a result of the oxidization of $Ce(OH)_3$ in alkaline condition. Moreover, $Ce(OH)_3$ is converted to CeO_2 in a dismutation solid state reaction [8, 27]. The main reactions which have been studied are as follows [8, 27, 28]:

$$H_2O + 1/2\ O_2 + 2\ e \rightarrow 2OH^- \quad (1)$$

$$Ce^{3+} + 3\left(OH^-\right) \rightarrow Ce(OH)_3 \quad (2)$$

$$2Ce(OH)_3 + 2\left(OH^-\right) \rightarrow 2CeO_2 + 4H_2O + 2e. \quad (3)$$

Cerium oxide and hydroxide block the cathodic sites and hinder the reduction reaction and, therefore, the corrosion rate is decreased. New cathodes are formed to counterbalance any anodic activity (dissolution) and the hindering process is perpetuated until all the cathodic sites become covered with cerium precipitates [29]. It has been found that these inhibitors are leached out slowly and show self-healing of defects [29]. Also, this mechanism can be performed in the best way if the concentration of the additive stays at its optimum value. The homogeneity of the film decreases at high concentrations of cerium, which leads to weaker corrosion protection properties [29].

SEM and EDX

SEM and EDX were used to study and analyze precipitates and elements such as cerium along the inscribed area of coatings. SEM analysis was performed after the immersion tests and showed the presences of CeO_2 deposit on the scratch areas of 4C2CN as depicted in Fig. 9a, b and 4C3CN in Fig. 9c–e. Figure 9e illustrates that the deposits on the scratch area are mostly needle like. This rosette morphology in coating may be related to the release of cerium inside defects, producing hydroxide or oxide precipitates when reacting with hydroxyl groups from cathodic reactions. Figure 10 indicates EDX analysis which confirms the presence of cerium in the scratched areas. This "self-healing" mechanism blocked defective areas and increased the compactness of the oxide layer. In addition, this process increased the resistance of this layer and, thus, provided a better protection of the coated substrate.

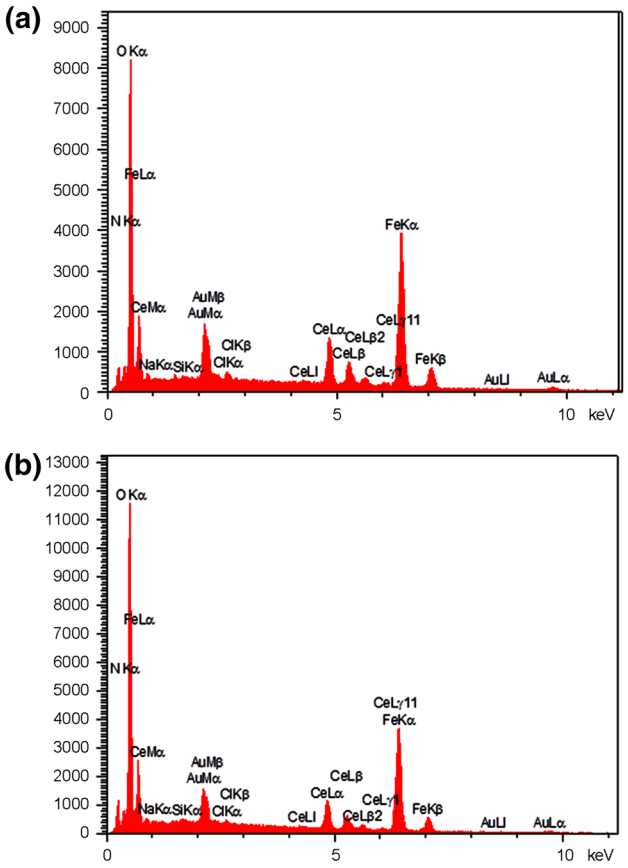

Fig. 10 EDX analysis from the scratch area for samples **a** 4C2CN and **b** 4C3CN

Conclusion

Epoxy nanocomposite coatings were provided by dispersion of MMT and CN using a mechanical agitation and sonication process. The results of FESEM and TEM showed that the cured nanocomposite 0C3CN produced non-continuous film that included several microcracks and pinholes. On the other hand, the clay particles in sample 4C0CN were dispersed and intercalated, but not fully exfoliated in the epoxy polymers. The obtained films with clay were less porous and more organized. Therefore, the clay addition to cerium nitrate improved the corrosion protection properties of these films. EIS analysis indicated that the addition of cerium nitrate to epoxy–clay led to prevention of the corrosion of carbon steel substrates and increased the resistance of a scratched area against corrosion. SEM images showed that the deposits in scratch area were mostly needle like. EDX analysis confirmed the presence of cerium migration into the defective sites.

References

1. Sabagh S, Bahramian AR, Mehrdad Kokabi M (2012) SiAlON nanoparticles effect on the corrosion and chemical resistance of epoxy coating. Iran Polym J 21:837–844

2. Ajami N, Bahrami Panah N, Danaee I (2014) Oxytetracycline nanosensor based on poly-*ortho*-aminophenol/multi-walled carbon nanotubes composite film. Iran Polym J 23:121–126
3. Sabagh S, Bahramian AR, Kokabi M (2012) SiAlON nanoparticles effect on the behaviour of epoxy coating. Iran Polym J 21:229–237
4. Jayamurgan P, Ponnuswamy V, Ashokan S, Mahalingam T (2013) The effect of dopant on structural, thermal and morphological properties of DBSA-doped polypyrrole. Iran Polym J 22:219–225
5. Shokrieh MM, Esmkhani M, Vahedi F, Shahverdi HR (2013) Improvement of mechanical and electrical properties of epoxy resin with carbon nanofibers. Iran Polym J 22:721–727
6. Bahrami Panah N, Payehghadr M, Danaee I, Nourkojouri H, Sharbatdaran M (2012) Investigation of corrosion performance of epoxy coating containing polyaniline nanoparticles. Iran Polym J 21:747–754
7. Motahari S, Dornajafi L, Fotovat Ahmadi I (2012) Migration of organic compounds from PET/clay nanocomposites: influences of clay type, content and dispersion state. Iran Polym J 21:669–681
8. Darmiani E, Danaee I, Rashed GR, Zaarei D (2013) Formulation and study of corrosion prevention behavior of epoxy cerium nitrate–montmorillonite nanocomposite coated carbon steel. J Coat Technol Res 10:493–502
9. Bahramian AR, Ahmadi LS, Kokabi M (2014) Performance evaluation of polymer/clay nanocomposite thermal protection systems based on polyethylene glycol phase change material. Iran Polym J 23:163–169
10. Nakhaei NR, Mostafa Arab NB, Naderi G (2013) Application of response surface methodology for weld strength prediction in laser welding of polypropylene/clay nanocomposite. Iran Polym J 22:351–360
11. Tianlan P, Ruilin M (2009) Rare earth and silane as chromate replacers for corrosion protection on galvanized steel. J Rare Earth 27:159–163
12. Wei X, Ruilin M, Chang M, Tianlan P (2010) Study on corrosion resistance of the BTESPT silane cooperating with rare earth cerium on the surface of aluminum-tube. J Rare Earth 28:117–122
13. Yan W, Zhang X, Zhu Y, Chen H (2012) Synthesis and characterization of self-crosslinkable zinc polyacrylate latices at room temperature. Iran Polym J 21:631–639
14. Darmiani E, Rashed GR, Zaarei D, Danaee I (2013) Synergistic effects of montmorillonite/cerium nitrate additives on the corrosion performance of epoxy–clay nanocomposite coatings. Polym-Plast Technol 52:980–990
15. Lee YL, Chu YR, Chen FJ, Lin CS (2013) Mechanism of the formation of stannate and cerium conversion coatings on AZ91D magnesium alloys. Appl Surf Sci 276:578–585
16. Brusciotti F, Snihirova DV, Xue H, Montemor MF, Lamaka SV, Ferreira MGS (2013) Hybrid epoxy–silane coatings for improved corrosion protection of Mg alloy. Corros Sci 67:82–90
17. Snihirova D, Lamaka SV, Montemor MF (2012) "SMART" protective ability of water based epoxy coatings loaded with $CaCO_3$ microbeads impregnated with corrosion inhibitors applied on AA2024 substrates. Electrochim Acta 83:439–447
18. Trabelsi W, Cecilio P, Ferreira MGS, Montemor MF (2005) Electrochemical assessment of the self-healing properties of Ce-doped silane solutions for the pre-treatment of galvanised steel substrates. Prog Org Coat 54:276–284
19. Montemor MF, Snihirova DV, Taryba MG, Lamaka SV, Kartsonakis IA, Balaskas AC, Kordas GC, Tedim J, Kuznetsova A, Zheludkevich ML, Ferreira MGS (2012) Evaluation of self-healing ability in protective coatings modified with combinations of layered double hydroxides and cerium molibdate nanocontainers filled with corrosion inhibitors. Electrochim Acta 60:31–40
20. Ferreira MGS, Duarte RG, Montemor MF, Simoes AMP (2004) Silanes and rare earth salts as chromate replacers for pre-treatments on galvanised steel. Electrochim Acta 49:2927–2935
21. Lim SR, Chow WS (2011) Fracture toughness enhancement of epoxy by organo-montmorillonite. Polym-Plast Technol Eng 50:182–189
22. Danaee I (2011) Kinetics and mechanism of palladium electrodeposition on graphite electrode by impedance and noise measurements. J Electroanal Chem 662:415–420
23. Danaee I, Noori S (2011) Kinetics of the hydrogen evolution reaction on NiMn graphite modified electrode. Int J Hydrogen Energy 36:12102–12111
24. Chico B, Galvan JC, de la Fuente D, Morcillo M (2007) Electrochemical impedance spectroscopy study of the effect of curing time on the early barrier properties of silane systems applied on steel substrates. Prog Org Coat 60:45–53
25. Sun L, Boo WL, Clearfield A (2008) Barrier properties of model epoxy nanocomposites. J Membr Sci 318:129–136
26. Gholami M, Danaee I, Maddahy MH, RashvandAvei M (2013) Correlated ab initio and electroanalytical study on inhibition behavior of 2-mercaptobenzothiazole and its thiole-thione tautomerism effect for the corrosion of steel (API 5L X52) in sulphuric acid solution. Ind Eng Chem Res 52:14875–14889
27. Cabral AM, Trabelsi W, Serra R, Montemor MF, Zheludkevich ML, Ferreira MGS (2006) The corrosion resistance of hot dip galvanized steel and AA2024-T3 pre-treated with bis-[triethoxysilylpropyl] tetrasulfide solutions doped with $Ce(NO_3)_3$. Corros Sci 48:3740–3758
28. Tavandashti NP, Sanjabi S (2010) Corrosion study of hybrid sol–gel coatings containing boehmite nanoparticles loaded with cerium nitrate corrosion inhibitor. Prog Org Coat 69:384–391
29. Lampke T, Darwich S, Nickel D, Wielage B (2008) Development and characterization of sol–gel composite coatings on aluminum alloys for corrosion protection. Mater Sci Eng Technol 39:914–919